

UNIVERSITY OF CRETE

MASTER THESIS

**Preparation of high-dimensional
maximally entangled states of a single
photon in a quantum walk**

Author:
Katerina Gratsea

Supervisors:
Prof. Maciej Lewenstein and
Dr. Alexandre Dauphin
(ICFO)

*A thesis submitted in fulfillment of the requirements
for the degree of Advanced Physics*

in the

Department of Physics
University of Crete

September 15, 2018

Acknowledgements

First of all, I would like to thank both my supervisors, Prof. Maciej Lewenstein and Dr. Alexandre Dauphin, for the vital help and guidance throughout this master thesis. I am grateful to all those with whom I had the pleasure to collaborate during this work. Specifically, the members of the group Maria Maffei, Albert Alloy, Manabendra Nath Bera, Emilio Pisanty and Swapan Rana for the beneficial discussions and feedback. Also, the members of Antonio Acin's group, Alexia Salavrakos, Osvaldo Jimenez Farias and Zahra Raissi.

Katerina Gratsea

Introduction

Quantum information theory has greatly evolved in recent years and offers advancements in many different fields, among them quantum walks [1]. The term *quantum walk* was first used in 1993 at the work of Y. Aharonov, L. Davidovich and N. Zagury [2].

Quantum walks are the generalization of classical random walks (CRWs). The CRW consists of a walker, an initial localized particle on a lattice, and of a coin operator. At each step, the coin is tossed and determines the direction in which the walker is moving. Each step of the walk consists of a coin toss and a movement of the walker. On the other hand, the quantum walks consists of two unitary operators: a shift operator and a coin operator. Contrary to the CRW where all operators are unitary and not random.

We should emphasize the different role of the coin operator in a CRW compared to the one in a QW. The coin operator generates the randomness in a CRW, while in a QW alters the amplitude distribution in the final state. Moreover, the final state of a QW has the feature of a quantum state; the final state could be a superposition of many discrete states. Therefore, the randomness in the quantum walks comes from the measurement of the final state and not from the coin operator [3].

The above description of QW belongs to the category of discrete-time quantum walks (DTQWs), while another category of QW is the continuous-time quantum walks (CTQWs). The difference comes from the evolution of the walk. The unitary evolution is time-dependent in the DTQW contrary to time-independent evolutions to CTRW. Generally in a QW, regardless the category, the unitary evolution remains the same throughout the walk [4]. Recently, though, there has been an increasing interest in dynamically disordered QWs (DDQWs), at which the unitary evolution is different at each step. These kind of walks are the ones that we are interested in at this work.

Quantum walks have many applications. In quantum simulators i.e. Floquet hamiltonians [5], band structures [6] and energy transport in chemical reactions [7]. Furthermore, QWs play an important role in quantum algorithms just like CRWs contribute to classical algorithms. Specifically, CRW are greatly useful in search algorithms and the same happens with QWs; examples of works are [8] and a recent review article [9]. Moreover, QWs have applications in quantum computation. Importantly, it was shown that any quantum algorithm could be reconstructed as a QW algorithm using a CTQW [10] and a DTQW [11]. Finally, QWs could be used for the preparation of arbitrary quantum states [12] and this capability is the one we investigate in this work; for the preparation of maximally entangled states.

Entanglement is a vital resource in quantum information and computation and single-photon entanglement is an active research field. There are different applications of single-photon quantum walks, such as simulation of the Brillouin zone [6]

and implementations in quantum computation [13]. We should emphasize that entanglement in a single-photon occurs between the different degrees of freedom of the particle, i.e. polarization, orbital angular momentum, time-bin energy and spatial mode. There are many measurements related to entanglement but we will restrict the work to the *Schmidt norms*; we bipartite the system to two subsystems and measure the correlations between them. This measurement, as will be proven in detail, is related to the *Renyi α entropy*.

In this work, we explore the preparation of single-particle maximally entangled states with respect to the aforementioned definition of the entanglement; the Schmidt norm. The bipartition of the system is between the spin and orbital angular momentum degrees of freedom. Additionally, we exploit the large size of the orbital angular momentum (OAM) Hilbert space to construct high-dimensional maximally entangled states, which gain increasing interest in the quantum information technologies in the recent years. Specifically, we use DTQWs because these quantum walks enhance the value of entanglement at the final state [14]. Chapter 1 is an introduction on QWs, entanglement, the numerical techniques used and the experimental realizations of quantum walks. Chapter 2 investigates the usefulness of the states prepared and related work. Then, we introduce two methods to prepare the states and a discussion on the results. Chapter 3 discusses the conclusion of the work.

Contents

Acknowledgements	iii
Introduction	vi
1 Theoretical background	3
1.1 Quantum walks on a line	3
1.1.1 Mathematical definition	3
1.2 Entanglement	4
1.2.1 Definition	4
1.2.2 Entanglement and Schmidt norm	5
1.2.3 Renyi α entropy and Schmidt norm	6
1.3 Numerical methods	7
1.3.1 minimization techniques : basin hopping	7
1.4 Experimental scheme	8
2 Generation of single particle maximally entangled states with a quantum walk	13
2.1 Introduction	13
2.1.1 Why are maximally entangled states useful ?	13
2.1.2 Preparation of maximally entangled states with a quantum walk	14
2.2 Algorithms to prepare maximally entangled states	15
2.2.1 Method A : Combination of two existing algorithms	15
Reuvers's algorithm	16
Algorithm for quantum state engineering with a quantum walk	21
Combination of the two algorithms	23
2.2.2 Method B: Quantum walk with gradient descent techniques	23
The algorithm	24
Numerical results	25
2.3 Discussion	27
3 Conclusions	29
A Appendix A : Proof of Reuvers's algorithm	31
B Appendix B : Numerical examples	33
B.1 Example of "backward" quantum walk	33
B.2 Examples of Method A : combination of both algorithms	33
B.2.1 Hilbert space of dimension 4	33
B.2.2 Hilbert space of higher dimensions	34
B.3 Examples of Method B : algorithm with optimization component	35
Bibliography	37

Chapter 1

Theoretical background

1.1 Quantum walks on a line

1.1.1 Mathematical definition

The quantum walk consists of n applications of a unitary operator U , which is itself a combination of a translation and a local rotation. We define the *step operator* $U = SC$ as the product of both the translation S and rotation C operators. The translations are introduced by shift operators S which move the walker according to the coin state. The walker is realised with a high-dimensional system spanned by $|k\rangle$, while the coin state is spanned by $|s\rangle = |\uparrow\rangle, |\downarrow\rangle$.

An initial state of the walker is described by

$$|\psi\rangle = \sum_{k=1}^n \sum_{s \in (\uparrow, \downarrow)} u_{k,s} |k\rangle \otimes |s\rangle \quad (1.1)$$

where k refers to the walker's sites and s to the coin states.

The conventional shift operators moves the walker either to the left or to the right regarding the coin state. The shift operator S is given by

$$S = \sum_k (|k-1\rangle\langle k| \otimes |\uparrow\rangle\langle\uparrow| + |k+1\rangle\langle k| \otimes |\uparrow\rangle\langle\uparrow|) \quad (1.2)$$

Other works introduce the one-directional shift operator for mathematical simplicity [12]; the walker stands still or moves right regarding the coin state as shown below

$$S = \sum_k (|k\rangle\langle k| \otimes |\uparrow\rangle\langle\uparrow| + |k+1\rangle\langle k| \otimes |\downarrow\rangle\langle\downarrow|). \quad (1.3)$$

The rotations are introduced by the coin operators C_i which are unitary transformations. The coin operators alter the way the amplitudes of the state are distributed, i.e. the weights at every site are redefined. Well-known examples of coin operators is the Hadamard operator

$$H = \frac{1}{\sqrt{2}} \begin{bmatrix} 1 & 1 \\ 1 & -1 \end{bmatrix} \quad (1.4)$$

which forms the simplest case of a quantum walk on a line [15]. The walker weights are equally distributed at the two coin states at each step since

$$H |\uparrow\rangle = \frac{1}{\sqrt{2}}(|\uparrow\rangle + |\downarrow\rangle) \quad (1.5)$$

$$H |\downarrow\rangle = \frac{1}{\sqrt{2}}(|\uparrow\rangle - |\downarrow\rangle). \quad (1.6)$$

Moreover, the coin operator could have the most general form of a SU(2) operator with three independent parameters ξ, ζ, θ .

$$C_n = \begin{bmatrix} e^{i\xi} \cos(\theta) & e^{i\zeta} \sin(\theta) \\ e^{-i\zeta} \sin(\theta) & -e^{-i\xi} \cos(\theta) \end{bmatrix} \quad (1.7)$$

where $\xi, \zeta \in [0, 2\pi]$ and $\theta \in [0, \pi/2]$ [15].

After one step the state reads

$$U |\psi\rangle \equiv S (C_1 \otimes I_{walker}) |\psi\rangle. \quad (1.8)$$

1.2 Entanglement

1.2.1 Definition

Entanglement is a property of a quantum system. Let us consider a division of a system in two subsystems A and B. A state is said entangled with respect the two subsystems A and B if it is not possible to write it in terms of a tensor product of states of the subsystems A and B.

Formally, we divide the Hilbert space H in two blocks H_A and H_B , $H_A \otimes H_B$. The quantum system, given by the quantum state $|\psi\rangle$, is not entangled when the state $|\psi\rangle$ can be written as a product state $|\psi\rangle = |\psi_A\rangle \otimes |\psi_B\rangle$. When the state can not be written as a product state then the subsystems A and B are entangled.

Consider the simplest case where each subsystem has dimension $d_i = 2$; the Hilbert space of each subsystem H_i is spanned by the states $\{|\uparrow_A\rangle, |\downarrow_A\rangle\}$. Then, the Hilbert space of the system H has dimension $d = 4$. Simple examples of not entangled states are

$$|\psi\rangle = |\uparrow_A \uparrow_B\rangle \quad (1.9)$$

$$|\psi\rangle = \frac{1}{\sqrt{2}} (|\uparrow_A \uparrow_B\rangle + |\uparrow_A \downarrow_B\rangle) = |\uparrow_A\rangle (|\uparrow_B\rangle + |\downarrow_B\rangle). \quad (1.10)$$

Examples of entangled states are

$$|\psi\rangle = \frac{1}{\sqrt{2}} (|\uparrow_A \uparrow_B\rangle \pm |\downarrow_A \downarrow_B\rangle) \quad (1.11)$$

$$|\psi\rangle = \frac{1}{\sqrt{2}} (|\uparrow_A \downarrow_B\rangle \pm |\downarrow_A \uparrow_B\rangle) \quad (1.12)$$

which form the well-known Bell states. [16]

It is useful to emphasize the geometric representation of the entanglement. As mentioned above, in the simplest case the Hilbert space has dimension $d = 4$ and is spanned by the states $|\uparrow_A \uparrow_B\rangle, |\uparrow_A \downarrow_B\rangle, |\downarrow_A \uparrow_B\rangle, |\downarrow_A \downarrow_B\rangle$. Then, the state of each subsystem can not be considered independent of the other. Specifically,

$$\frac{|\uparrow_A \uparrow_B\rangle + |\downarrow_A \downarrow_B\rangle}{\sqrt{2}} \neq \frac{|\uparrow_A + \downarrow_A\rangle}{\sqrt{2}} \frac{|\uparrow_B + \downarrow_B\rangle}{\sqrt{2}} = \frac{|\uparrow_A \uparrow_B\rangle + |\uparrow_A \downarrow_B\rangle + |\downarrow_A \uparrow_B\rangle + |\downarrow_A \downarrow_B\rangle}{2} \quad (1.13)$$

The states $\frac{|\uparrow_A \uparrow_B\rangle + |\downarrow_A \downarrow_B\rangle}{\sqrt{2}}$ and $\frac{|\uparrow_A + \downarrow_A\rangle}{\sqrt{2}} \frac{|\uparrow_B + \downarrow_B\rangle}{\sqrt{2}}$ correspond to different vectors of the Hilbert space [17].

The subsystems A and B should refer to two different degrees of freedom of the system. One could examine the entanglement of a system of two photons, at which the polarization of each photon corresponds to one of the two subsystems A and B . Recently, however, the entanglement between different degrees of freedom for each photon is explored, i.e. polarization of photon A and orbital angular momentum of photon B . This is called *hybrid entanglement*

$$|\psi_{hyb}\rangle = \frac{1}{\sqrt{2}}(|L, 0\rangle_A |H, 2\rangle_B + |R, 0\rangle_A |H, -2\rangle_B). \quad (1.14)$$

where A and B refer to the first and second photon, R, L, H and V , refer to right, left, horizontal and vertical polarization respectively, while 0 and ± 2 refer to the orbital angular momentum of the photon [18]. Hybrid entanglement could also be referred to different degrees of freedom of a single photon. One of the degrees of freedom could be polarization, orbital angular momentum, position, frequency and time. An example, with OAM and polarization is

$$|\psi_{hyb}\rangle = \frac{1}{\sqrt{2}}(|2, H\rangle + |-2, V\rangle). \quad (1.15)$$

In the latter case, entanglement is distributed in different degrees of freedom. When two photons are simultaneously entangled in different degrees of freedom, the entanglement is called *hyper entanglement* [18]

$$|\psi_{hyb}\rangle = \frac{1}{\sqrt{2}}(|H, H\rangle + |V, V\rangle)_{pol} \otimes (|s, s\rangle + |l, l\rangle)_{time} \otimes (|-1, 1\rangle + |0, 0\rangle + |1, -1\rangle)_{OAM}. \quad (1.16)$$

1.2.2 Entanglement and Schmidt norm

As mentioned above, in order to investigate the entanglement of a quantum system, we must divide the system into two subsystems. Then, the quantum system described by the quantum state $|\psi\rangle$ can be written in the form

$$|\psi\rangle = \sum_m \sum_n A_{m,n} |\psi_m^A\rangle |\psi_n^B\rangle \quad (1.17)$$

where the $|\psi_m^A\rangle$ and $|\psi_n^B\rangle$ are orthonormal bases in the two Hilbert subspaces.

Let us emphasize that in Eq. (1.17) we have a double summation over m and n .

One could apply the singular-value decomposition on the matrix $A_{m,n}$ and transform it to a product of three matrices

$$\mathbf{A} = \mathbf{U}\mathbf{D}\mathbf{V}' \quad (1.18)$$

where \mathbf{U} is square and unitary, \mathbf{D} diagonal and \mathbf{V}' rectangular with orthonormal rows. This gives

$$|\psi\rangle = \sum_{m,n,k} U_{m,k} D_{k,k} V'_{k,n} |\psi_m^A\rangle |\psi_n^B\rangle \quad (1.19)$$

Defining $|\phi_n^A\rangle = \sum_m U_{m,n} |\psi_m^A\rangle$, $|\phi_n^B\rangle = \sum_m V'_{m,n} |\psi_m^B\rangle$ and $D_{n,n} = \lambda_n$, the state $|\psi\rangle$ is written

$$|\psi\rangle = \sum_n \lambda_n |\phi_n^A\rangle |\phi_n^B\rangle \quad (1.20)$$

This was proposed by Schmidt in 1907 and is called the Schmidt decomposition[19]. The orthonormal states $|\psi_m^A\rangle$ and $|\psi_n^B\rangle$ have been transformed to new orthonormal states $|\phi_n^A\rangle$ and $|\phi_n^B\rangle$. Here, the main difference is that the state $|\psi\rangle$ is described by a single sum, which is restricted by the smaller Hilbert subspace $k \leq \min(d_A, d_B)$.

The elements λ_k satisfy the condition $\sum |\lambda_k|^2 = 1$, for a normalized state $|\psi\rangle$. Entanglement is encoded in the so-called *Schmidt coefficients* λ_k , with the following extreme cases:

- $\lambda_1 = 1, \lambda_k = 0$ for $k > 1$: only one term survives, which results in product state and no entanglement
- $\lambda_k = \lambda$ for all k : all terms with equal weight, which results in a maximal entanglement. [20]

1.2.3 Renyi α entropy and Schmidt norm

Renyi α entropy for a density matrix ρ , $S_\alpha(\rho)$, is a generalization of the von Neumann entropy $S(\rho)$. In the limit that α reaches one, the Renyi entropy becomes equivalent to the von Neumann entropy

$$S(\rho) = \text{Tr}[-\rho \log \rho] = \lim_{\alpha \rightarrow 1} S_\alpha(\rho). \quad (1.21)$$

The Renyi α entropy for a density matrix ρ (for $\alpha \geq 0$ and $\alpha \neq 1$) is defined as

$$S_\alpha(\rho) \equiv \frac{1}{1-\alpha} \log(\text{Tr}[\rho^\alpha]) \quad (1.22)$$

The definition of *Schmidt norms* are

$$\| |\psi\rangle \|_{p,k} = \left(\sum_{i=1}^k (\lambda_i^\Psi)^p \right)^{1/p} \quad (1.23)$$

where $k \leq \min(d_A, d_B)$ and $p \geq 1$.

The Renyi α entropy could be related to the Schmidt norm as follow [21]

$$S_a(\rho) \equiv \frac{2\alpha}{1-\alpha} \log(\|\psi\|_{2\alpha,k}) \quad (1.24)$$

Here comes the proof of the above statement. The quantum system $|\psi\rangle$ can be reduced to system A

$$\rho_A^\psi \equiv \text{Tr}_B[|\psi\rangle\langle\psi|] = \sum_{i=1}^k (\lambda_i^\Psi)^2 |\psi_A^i\rangle\langle\psi_A^i| \quad (1.25)$$

for $k \leq \min(d_A, d_B)$ where $S(\rho_A^\psi)$ is the *entanglement entropy* of one of the reduced density operators. Then, we can arrive to the following equation

$$\text{Tr}_A \left(\rho_A^\psi \right)^{p/2} = \sum_{i=1}^k (\lambda_i^\Psi)^p \quad (1.26)$$

With the help of Eqs. (1.23) and (1.26), we find

$$\|\psi\|_{p,k}^p = \text{Tr}_A \left(\rho_A^\psi \right)^{p/2} \quad (1.27)$$

Then, for $p = 2\alpha$ the above equation becomes

$$\|\psi\|_{2\alpha,k}^{2\alpha} = \sum_{i=1}^k (\lambda_i^\Psi)^\alpha \quad (1.28)$$

and equation (1.22) becomes

$$S_a(\rho) \equiv \frac{2\alpha}{1-\alpha} \log(\|\psi\|_{2\alpha,k}) \quad (1.29)$$

1.3 Numerical methods

1.3.1 minimization techniques : basin hopping

Throughout this work, the global maximum of a function was needed. In order to overcome this task we used the *basin-hopping* algorithm provided by the *scipy* library in *python*. This function is a combination of both a simulated annealing component, due to the temperature parameter, and a gradient descent optimization component, due to the BFGS minimization method.

This algorithm is a stochastic algorithm which aims to find the global minimum of a function. Generally, in a stochastic global optimization problem, it is difficult to find the global minimum of the function. The algorithm runs for a number of different starting points and returns the lowest minimum found. The number of different starting points is determined by the parameter n_{iter} which value is set by the user. Additionally, there is the option $n_{iter,success}$, which is determined once again by the user, and stops the algorithm if the value of the minimum does not alter for the number of $n_{iter,success}$. Also, this algorithm includes a *temperature parameter* T (simulated annealing) which determines the jumps between the starting points of the iterations. For better results, it is suggested to be set equal to the difference in function value between the local minima.

Moreover, the algorithm allows the selection of the minimization technique. In this work, we selected as a minimization method the Broyden-Fletcher-Goldfarb-Shanno algorithm (BFGS). This is a quasi-Newton method proposed independently by four researchers Broyden, Fletcher, Goldfarb and Shanno in 1970. The importance of the method is that instead of computing analytically the Hessian of the function H_n^{-1} at step n , it uses gradient descent component to update the Hessian using the value of the Hessian at the previous step $n - 1$.

In more detail, in an optimization problem the local minimum x is determined as $x_{n+1} = x_n - \alpha H^{-1}g$ with α arbitrary, g the gradient and H the hessian of the function. According to Newton's method, the gradient and the Hessian of a function at point x are determined through the ∇f and $\nabla^2 f$ respectively. On the contrary with the BFGS method, where the Hessian is updated from the previous value of the Hessian and, hence, reducing the number of calculations by the algorithm.

Specifically, in the BFGS method we define $y_n = \nabla f(x_{n+1}) - \nabla f(x_n)$, $s_n = x_{n+1} - x_n$ and impose the second condition $H_{n+1}s_n = y_n$. The Hessian is defined as $H_{n+1} = H_n + \alpha uu^T + \beta vv^T$, where $u = y_n$ and $v = H_n s_n$. Then, using the second condition, we find the values of α and β and the equation of the Hessian becomes

$$H_{n+1} = H_n + \frac{1}{y_n^T s_n} uu^T - \frac{1}{s_n^T H_n s_n} \beta vv^T = H_n + \frac{y_k y_k^T}{y_n^T s_n} - \frac{H_n s_n s_n^T H_n^T}{s_n^T H_n s_n} \quad (1.30)$$

Thus, the Hessian H_n is a function of H_{n-1}, y_n and s_n [22].

1.4 Experimental scheme

Quantum walks have been realized in optics, photonic crystals, cold atoms [23], [24]. We here focus on the realization of a photonic QW. The first experimental schemes of 1D quantum walks were facing the problem of a quickly growing number of optical elements needed for the implementation and lead to instability. In 2007 the experimental realization became simpler by using Mach-Zehnder interferometers but the instability remained still a problem due to the interferometers [25]. Then, at 2010 the stability and the number of optical elements were significantly improved by using birefringent calcite [26]. Moreover, in 2010 another experimental implementation was proposed by [13]. They replaced the Mach-Zehnder interferometer with a q-plate (QP), which makes the system simpler and more efficient. Also, the stability of the scheme is better compared to the proposal of [26].

In the paper [13], they proposed the following experimental scheme 1.1.

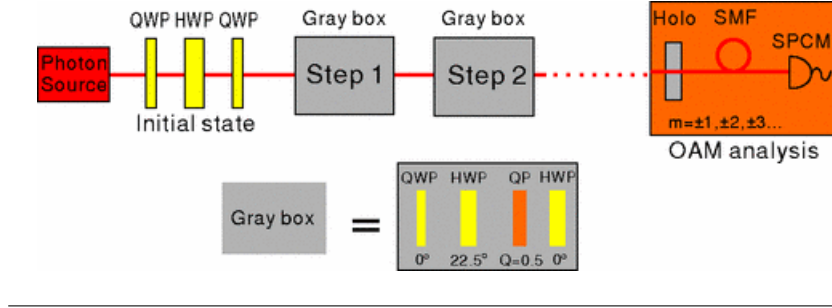


FIGURE 1.1: Proposal of experimental scheme [13]

A photon is emitted from the photon source (red colour) and the first three plates (yellow colour) allow the preparation of the state to a desired superposition. Each step of the quantum walk is realized by a gray box and, hence, the n number of steps are realized with n grey boxes. The first two plates inside the gray box realize the coin operator (for an example they discuss the Hadamard coin operator) and the rest, the conventional shift operator. At this point, we should underline that the unidirectional shift operator discussed in [12] does not have a direct experimental implementation. It is only used for mathematical simplicity but for experimental realizations the unidirectional shift operator should be altered to the both-directional one. Finally, the orange box is used for the analysis of the state with a computer generated hologram. The final state is a quantum superposition of different OAM sites $m = \pm 1, \pm 2, \dots, \pm n$. Then, in order to detect the OAM site m , a hologram of $-m$ is applied to the photon and the site m is changed to 0. The single-mode fiber (SMF) only allows the $m = 0$ OAM mode to pass through it and absorbs the rest of OAM sites. At the end of the SMF, the photon is detected by a single-photon count modulator (SPCM). By repeating this procedure with many photons, it is possible to detect the probabilities of each OAM site $|m\rangle$. A linear polarizer could be added before the orange box for the projective measurement in the spin angular momentum (SAM) space. With the above proposal, both the preparation and measurement of the states is experimentally feasible.

The first implementation of the aforementioned experimental proposal was realised in 2015 [6]. The experimental scheme is presented in the Fig. 1.2.

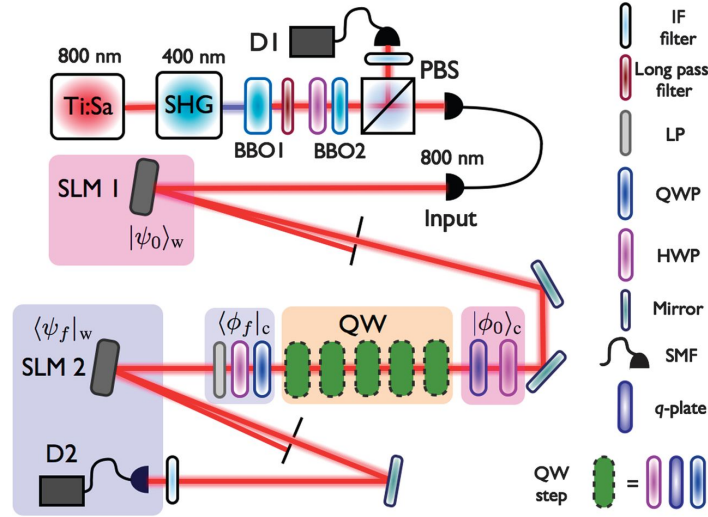


FIGURE 1.2: Implementation of experimental scheme [6]

The first row of Fig. 1.2 is needed for the preparation of a photon-pair, where photon A is detected (black line /) and only photon B enters the quantum walk (row 3). Before entering the QW, a SLM could be used for preparing the initial state in an arbitrary superposition of OAM sites. Moreover, a set of half-wave plates (HWP) and a quarter-wave plates (QWP) could be used for a generic preparation of the state over the SAM space $|\phi_0\rangle_c = \alpha |L\rangle + \beta |R\rangle$.

The coin operator is realized by a set of QWP and/or HWP, contrary to the shift operator which is realized by a QP

$$\begin{aligned} Q_\delta |L, m\rangle &= \cos(\delta/2) |L, m - 2q\rangle - i \sin(\delta/2) |R, m + 2q\rangle \\ Q_\delta |R, m\rangle &= \cos(\delta/2) |R, m\rangle - i \sin(\delta/2) |L, m - 2q\rangle \end{aligned} \quad (1.31)$$

where δ is the optical birefringent phase-retardation and q is the topological charge of the QP. Throughout our work, we choose to work with $q = 1/2$ and $\delta = \pi$.

After the QW, the state is projected in the SAM space with a combination of HWP-QWP along with a linear polarizer. Then, an SLM is used for the OAM analysis as described above.

The implementation of the above experiment was successful with an agreement equal or higher than 95% between the measured and the predicted probability distributions.

f

Chapter 2

Generation of single particle maximally entangled states with a quantum walk

2.1 Introduction

The goal of this thesis is the preparation of maximally entangled states between the polarization and orbital angular momentum of a single photon with a quantum walk.

2.1.1 Why are maximally entangled states useful ?

The core of quantum information technologies is based on the superposition and entanglement, a unique superposition, of quantum states. Although the role of entanglement in quantum algorithms is not yet clarified, it definitely plays a vital role in the architecture of quantum technologies; mainly for efficiently transferring information around with quantum teleportation protocols [27]. In this context, the preparation of the maximally entangled states is of high importance for the applications of quantum technologies.

Over the last decades, photonic quantum information has greatly advanced and already offers the first technological applications [4]. Lately single-particle entanglement, and specifically single-photon entanglement, has attracted a great interest[28].

Single-photon entangled states can be realized by using different degrees of freedom such as polarization, orbital angular momentum, spatial degree of freedom, etc. For example, the simplest case is the ququarts, a four dimensional system, that encodes 2 bits of information ($|0\rangle = |00\rangle$, $|1\rangle = |01\rangle$, $|2\rangle = |10\rangle$, $|3\rangle = |11\rangle$). Single-photon entangled states have the advantage that they can encode more information at a single particle level. Generally, the restriction to two dimensional systems is only technological [29] and recently, different schemes for the preparation of hybrid maximally entangled states have been proposed. They include the polarization and spatial degrees of freedom [30].

The preparation of high dimensional single photon entangled states is therefore of great interest. One implementation would be the simultaneous exploitation of the different degrees of freedom of a single photon. Another implementation is by taking advantage of the fact that the large size of the OAM Hilbert space [29]. The OAM internal degree of freedom is not restricted in the number of sites/states which

span the Hilbert space, contrary to the polarization which consists only of two states $\{\uparrow, \downarrow\}$. Moreover, since it is an "inner" degree of freedom of the photon compared to for example the spatial degree of freedom, it could be expanded to a large number of sites in a experimentally controlled way.

In this work, we explore the preparation of maximally entangled states between the polarization and orbital angular momentum of a single photon with a quantum walk. Moreover, we exploit the OAM internal degree of freedom and investigate the preparation of high-dimensional maximally entangled states between the polarization and orbital angular momentum of a single photon with a quantum walk.

Significantly, quantum C-NOT gates for single-photon two qubit quantum logic utilizing polarization and orbital angular momentum have already been proposed experimentally [31],[32] and along with single qubit gates allow the implementation of universal quantum computation. Our work provides the preparation of maximally entangled single photon states that could be used along with the above gates for photonic quantum information technologies.

It was recently shown for the first time that both degrees of freedom of an arbitrary state could be teleported by encoding the bits in a single photon [33]. Before that experiment, it was only possible to teleport only one degree of freedom. In the first realization of the experiment, both degrees of freedom teleported are two dimensional. The degrees of freedom used were the polarization and OAM of a single photon. It would be of great interest to expand the technique and to be able to teleport at the same time different degrees of freedom living in a higher dimensional space. As it is already mentioned above, the restriction to two dimensional systems is only technological [29]. In our work, we propose a way to prepare both hybrid Bell states and high-dimensional maximally entangled states between the polarization and OAM of a single photon with a quantum walk, which could be later used for quantum teleportation protocols; allowing larger amount of information to be transferred.

2.1.2 Preparation of maximally entangled states with a quantum walk

Starting from the maximally entangled state

$$|\psi_0\rangle = \frac{1}{\sqrt{2}}(|0, \uparrow\rangle + |0, \downarrow\rangle) \quad (2.1)$$

where the 0 refers to $m = 0$ orbital angular momentum and \uparrow, \downarrow represent the left and right polarization, other maximally entangled states could be generated by using the conventional shift operator and the identity coin operator, i.e. the evolution $U = S(I_{\text{coin}} \otimes I_{\text{OAM}})$

After one step and two steps of the quantum walk, we arrive at

$$|\psi_1\rangle = \frac{1}{\sqrt{2}}(|-1, \uparrow\rangle + |1, \downarrow\rangle) \quad (2.2)$$

and

$$|\psi_2\rangle = \frac{1}{\sqrt{2}}(|-2, \uparrow\rangle + |2, \downarrow\rangle) \quad (2.3)$$

maximally entangled states respectively. This could be implemented m times for the preparation of the arbitrary maximally entangled state

$$|\psi_m\rangle = \frac{1}{\sqrt{2}}(|-m, \uparrow\rangle + |m, \downarrow\rangle). \quad (2.4)$$

Moreover, one could start from the quantum states $|\psi_H\rangle = |0, \uparrow\rangle$ or $|\psi_V\rangle = |0, \downarrow\rangle$ and implement the evolution $U = S(H \otimes I_{OAM})$, where H is the well-known Hadamard operator (Eq. (1.4)) for the generation of a maximally entangled state. After the implementation of the Hadamard operator we arrive at

$$(H \otimes I_{OAM}) |\psi_0\rangle = \frac{1}{\sqrt{2}}(|0, \uparrow\rangle \pm |0, \downarrow\rangle) \quad (2.5)$$

where $|\psi_0\rangle$ is $|\psi_H\rangle$ and $|\psi_V\rangle$ respectively. Then, by applying the conventional shift operator we arrive at the maximally entangled state

$$|\psi_1\rangle = S(H \otimes I_{OAM}) |\psi_0\rangle = \frac{1}{\sqrt{2}}(|-1, \uparrow\rangle \pm |1, \downarrow\rangle) \quad (2.6)$$

where $|\psi_0\rangle$ is $|\psi_H\rangle$ and $|\psi_V\rangle$ respectively. But if this quantum walk evolves for more steps the resulting states are not maximally entangled [3].

It was shown that by randomly altering the coin operators at each step, maximally entangled states could asymptotically be achieved [14]. At their paper, *Rigolin et. al.* propose two different methods of preparing asymptotically maximally entangled states. The first method is by randomly choosing with a coin flip between the Hadamard coin operator (Eq.1.4) and the Fourier/Kempe coin operator

$$H = \frac{1}{\sqrt{2}} \begin{bmatrix} 1 & i \\ i & -1 \end{bmatrix}. \quad (2.7)$$

The second consists in randomly choosing the three parameters of the coin operators over three different uniform distributions. Starting with an arbitrary initial state and applying both quantum walks for a large number of steps ($n = 300$) result in the generation of a maximally entangled state. This maximally entangled state is not a Bell-state as the ones prepared above, but a high-dimensional state over many OAM sites of the state.

2.2 Algorithms to prepare maximally entangled states

2.2.1 Method A : Combination of two existing algorithms

Initially, we merge two already existing algorithms to generate maximally entangled states. The first algorithm finds a maximally entangled state starting from a random initial state [21]. More specifically, it maximizes the Rényi α entropy for a specific bipartition of the system. Though, the algorithm converges to a fixed point that may or may not be the global maximum. The second finds the required operators for the experimental realization of a desired state (in our case maximally entangled state) with a quantum walk [12]. The quantum walk consists of n discrete rotations (coin operators) and fixed translations (shift operators). The algorithm particularly provides a method to efficiently compute the set of coin parameters. Thus, the first approach

consists of combining the two algorithms and adding a simulated annealing component to overcome the above stated problem of finding the global maximum at the algorithm of [21]. As a result, we will have a concrete algorithm that will take as input a random initial state and give as an output a maximally entangled state with respect to the aforementioned definition.

Reuvers's algorithm

Reuvers's algorithm is one of the two existing algorithms that we will need for the preparation of the aforementioned states. The role of this algorithm is to find the desired maximally entangled states.

Goal of the algorithm Given any initial state $|\psi\rangle \in H_A \otimes H_B$, the goal of the algorithm is to reach a state $|\psi'\rangle$ with higher value of entanglement between the two parts belonging in H_A and H_B respectively.

The algorithm The algorithm consists of two main steps, repeated Schmidt decomposition and projection in a selected subspace $U \subset H_A \otimes H_B$. The algorithm suggested by Reuvers [21] has the following steps:

1. Start with an arbitrary initial state $|\psi\rangle \in H_A \otimes H_B$ with $P|\psi\rangle = |\psi\rangle$. P is the projector onto a subspace U and satisfies the conditions $P^\dagger = P, P^2 = P, \text{Im}(P) = U$. $\text{Im}(P)$ refers to the column space (or range or image) of a matrix P , which is the span of its column vectors. Therefore, the last condition just guarantees that P projects to the whole subspace of U and not a part of it.
2. Apply Schmidt decomposition to $|\psi\rangle$, as discussed in Sec. 1.2.2
3. Define the normalized vector

$$|\varphi\rangle := \frac{P \left(\sum_{i=1}^k (\lambda_i^\psi)^{p-1} |\psi_A\rangle \otimes |\psi_B\rangle \right)}{\| P \left(\sum_{i=1}^k (\lambda_i^\psi)^{p-1} |\psi_A\rangle \otimes |\psi_B\rangle \right) \|} \quad (2.8)$$

4. Redefine $|\psi\rangle := |\varphi\rangle$ and repeat from 2.

It can be proven (see Appendix A) that the above procedure leads to a global or local maximum of the *Schmidt norm*

$$\| |\psi\rangle \|_{p,k} = \left(\sum_{i=1}^k (\lambda_i^\psi)^p \right)^{1/p} \quad (2.9)$$

where $k \leq \min(d_A, d_B)$ and $p \geq 1$.

As explained in Chapter 1, entanglement is encoded in the Schmidt coefficients λ_i (see Sec. 1.2.2) and the Schmidt norm is related with the Renyi α entropy (see Sec. 1.2.3) with $\alpha = p/2$. At the case where $p = 1$ and $k = \min(d_A, d_B)$, the Schmidt norm is equal to 1 for a separable state and equal to \sqrt{k} for a maximally entangled state. Throughout this report p is assumed to be equal to 1.

Numerical implementation In the simplest case, the Hilbert space $H \equiv H_A \otimes H_B$ has dimension $d = d_A * d_B = 4$, since the dimension of each subsystem of qubits is $d_i = 2$. An arbitrary initial state of the system is given by

$$|\psi_{in}\rangle = a|00\rangle + b|10\rangle + c|01\rangle + d|11\rangle \quad (2.10)$$

Then, a 2-dimensional subspace U of H is spanned by two vectors v_1 and v_2 . From these vectors, we form a matrix A

$$A = [v_1 \ v_2]. \quad (2.11)$$

Next, the projector operator is derived as

$$P = A(A^T A)^{-1} A^T \quad (2.12)$$

The matrix P satisfies all the conditions mentioned before. The condition $Im(P) = U$ is also satisfied since P and A have the same rank.

Next, we define the initial state of the algorithm as

$$|\psi\rangle = \frac{P|\psi_{in}\rangle}{\|P|\psi_{in}\rangle\|} \quad (2.13)$$

and we implement the steps 2, 3, 4 of the algorithm. Whether or not we are going to reach the global maximum of the *Schmidt norm*, mainly depends on the choice of the projector.

Finding the projectors By randomly selecting the subspace and forming the projector, it is not guaranteed that we will find the maximally entangled states (which are the global maximum of the algorithm). For some choices of the projector, the algorithm gets stacked to local minima (fixed points). The author [21] suggests that one could try to overcome this problem by adding a simulated annealing component to the algorithm. The algorithm outputs both Bell states and high-dimensional maximally entangled states and, for the reasons mentioned above, it would be of great interest to overcome this problem. We use the BFGS technique described in Sec.1.3.1 to bypass this problem and find the correct projectors which maximize the *Schmidt norm*.

In our case, the function that will be minimized is $F = norm - \sqrt{d}$, where *norm* is the Schmidt norm computed numerically from Eq. 1.23 with $p = 1, k = \min(d_A, d_B)$ and \sqrt{d} is its maximum value, $d = \min(d_A, d_B)$. The free variables to be determined are the matrix elements of the subspace. At this point, we should emphasize that Reuvers algorithm works only when at least one of the subsystems is of dimension $d = 2$. (see Appendix 2.1 for a proof of this result). This does not impose a problem for our purpose; since the subsystems are the polarization and orbital angular momentum of a single photon and the polarization always lives in a two dimensional space.

In the following plots, we will present how the algorithm converges to the maximum value $\sqrt{2}$. We should emphasize that there are two different iterations in the algorithm. The first one is the iterations of the Reuvers's algorithm, i.e the repeated Schmidt decomposition. This is manually set to 50. The second one is the iterations that are needed from the minimization function to reach the global maximum.

Firstly, we plot the simplest case that the OAM has only two sites. Figures 2.1 and 2.2 present the different iterations of the Reuvers's and the algorithm's respectively. From the figure 2.1, we can observe the validity of the Reuvers's algorithm; after each iteration, the value of the Schmidt norm is increased until it gets stucked. In the figure 2.2, we can clearly observe these points. The algorithm moves away from these local minima by using the temperature parameter, which in our case was set equal to one. The rest of the parameters had the following values : $n_{iter} = 10$, $n_{iter,success} = 2$.

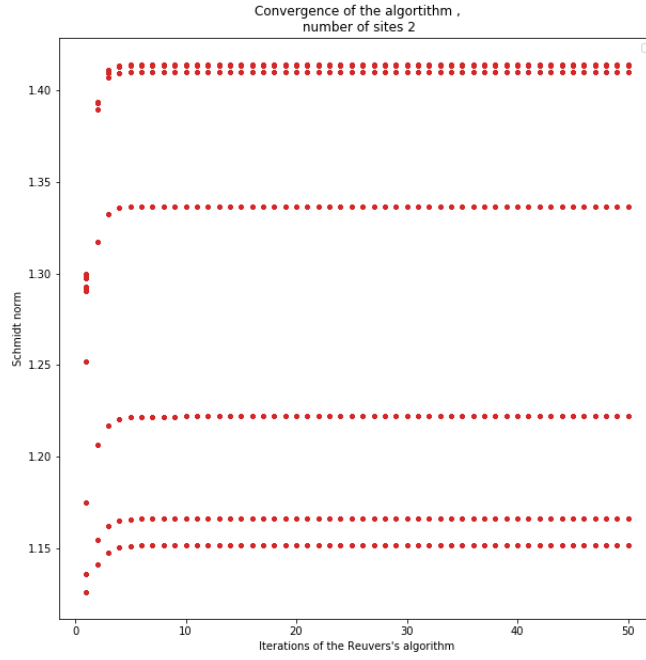


FIGURE 2.1: Result of the Reuver's algorithm with an optimization component for the case of a four-dimensional space with degrees of freedom the polarization and the two-dimensional orbital angular momentum. The x-axis represent the iterations of the Reuvers's algorithm.

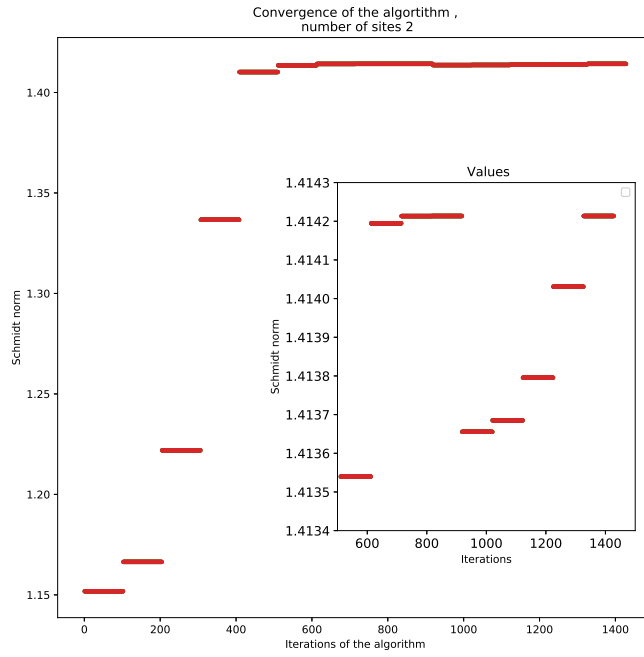


FIGURE 2.2: Result of the Reuver's algorithm with an optimization component for the case of a four-dimensional space with degrees of freedom the polarization and the two-dimensional orbital angular momentum. The x-axis represent the iterations of the minimization component.

Moreover, we should emphasize that both iterations do not have any physical meaning. They are the internal iterations that the algorithm performs until it reaches to the global maximum. After finish running, the algorithm gives as an output the state that better maximizes the Schmidt norm. This is what has the physical meaning and at what we are interested in. It is also possible to retrieve other states that are not maximally entangled but just entangled.

Next, we plot the results for $m = 25$ sites with iterations of Reuvers's in Fig.2.3 and the algorithm's in Fig.2.4. Once again, we obtain the same conclusion as the ones mentioned above. The only difference we could highlight is the number of iterations needed from the algorithm. In the case of $m = 25$ sites, we have 2500 iterations in contrast to the case of two sites where we have 1400 iterations. Although this does not impose any problems since as already mentioned these iterations do not have any physical meaning.

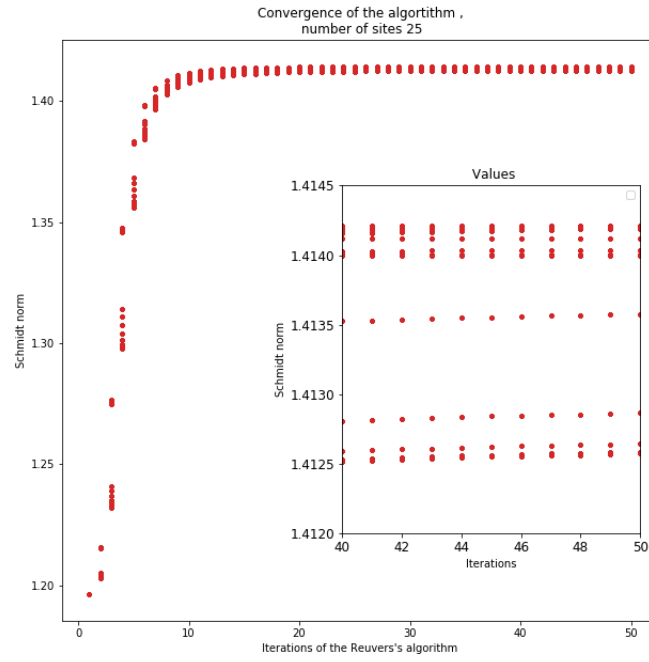


FIGURE 2.3: Result of the Reuver's algorithm with an optimization component for the case of a 50-dimensional space with degrees of freedom the polarization and the 25-dimensional orbital angular momentum. The x-axis represent the iterations of the Reuvers's algorithm.

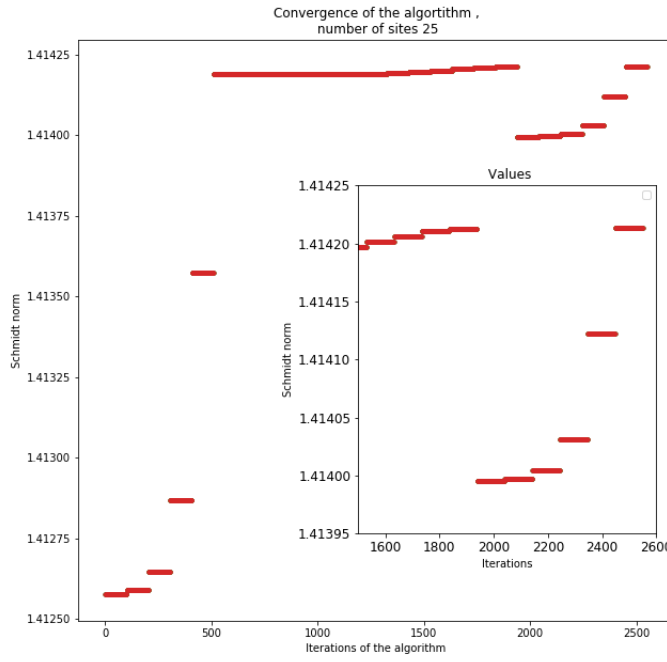


FIGURE 2.4: Result of the Reuver's algorithm with an optimization component for the case of a 50-dimensional space with degrees of freedom the polarization and the 25-dimensional orbital angular momentum. The x-axis represent the iterations of the minimization component.

Algorithm for quantum state engineering with a quantum walk

Goal of the algorithm In the paper of Ferraro et. al. [12] it is shown that coined quantum walks can be used for quantum state engineering of arbitrary superpositions of the walker's sites. The goal of this algorithm is to find the required operators for the experimental realization of a desired state over the walker's sites.

The quantum walk For mathematical simplicity, the authors define the unidirectional shift operator as in Eq. (1.2), while the set of coin operators are defined

$$C_N = N \begin{bmatrix} u_{1,\uparrow} & e^{i\alpha} u_{n,\uparrow} \\ u_{2,\downarrow} & e^{i\alpha} u_{n+1,\downarrow} \end{bmatrix} = N \begin{bmatrix} u_{1,\uparrow} & -e^{i\alpha} u_{2,\downarrow}^* \\ u_{2,\downarrow} & e^{i\alpha} u_{1,\uparrow}^* \end{bmatrix} \quad (2.14)$$

where $u_{k,s}$ refer to the elements of the state defined in Eq.(1.1); k refers to the walker's sites and s to the coin states. The coin operators alter the way the amplitudes of the state are distributed, i.e. the weights at every site are redefined.

The *step operator* is defined as the tensor product of both the coin and shift operator $W_C = S \otimes C$. Whenever an arbitrary state spanning over n sites is evolved with the step operator W_C , the resulting state spans over $n + 1$ sites and satisfies the conditions

$$\langle 1, \downarrow | \Psi \rangle = \langle n+1, \uparrow | \Psi \rangle = 0 \quad (2.15)$$

Moreover, the authors prove that evolving any state for n number of steps ($n > 1$), $|\Phi\rangle = W_{C_N} \dots W_{C_2} W_{C_1} |\Psi_{in}\rangle$ also satisfies the condition

$$\sum_{i=1}^s u_i^{(n)\dagger} u_{n-s+i}^{(n)} = 0 \quad (2.16)$$

Therefore, by defining the coin operators as in Eq. (2.14), the resulting state after n number of steps ($n > 1$), satisfies the two conditions (2.15) and (2.16).

Then, the final state $|\Phi\rangle$ can be projected to the state $|+\rangle = \frac{|\uparrow\rangle + |\downarrow\rangle}{\sqrt{2}}$, such that $|+\rangle \langle +| \phi \rangle \otimes |+\rangle$.

Throughout this work, the final state of the quantum walk will be referred as $|\Phi\rangle$ while the state after projection as $|\phi\rangle$.

The algorithm The above quantum walk (mentioned in this work as "forward" quantum walk) can be realized in the "backward" direction, i.e. starting from the final superposition of the $n+1$ walkers sites and reaching an initial state localised at the site $i=1$.

In this case, the initial state $|\phi\rangle$ is an arbitrary superposition of $n+1$ walkers sites with amplitudes $u_k \equiv \langle k | \phi \rangle$. But the final state of the quantum walk has to satisfy the conditions of Eqs. (2.15) and (2.16). Thus, the way of finding $|\Phi\rangle$ from $|\phi\rangle$ is by parametrizing $|\Phi\rangle$ as follow

$$|\Phi\rangle = N \left(u_1 |1, \uparrow\rangle + u_{n+1} |n+1, \downarrow\rangle + \sum_{i=2}^n [(u_i - d_i)] |i, \uparrow\rangle + d_i |i, \downarrow\rangle \right) \quad (2.17)$$

where the set of parameters $d_{i=2}^n$ have to be obtained and N is a renormalization constant. These parameters are determined by solving the following non-linear system of equations

$$\sum_{i=1}^n (u_i - d_i)^* (u_{n-s+i} - d_{n-s+i}) + d_{i+1}^* d_{n-s+i+1} = 0 \quad (2.18)$$

for every $s = 1, \dots, n-1$ with $d_1 = 0$ and $d_{n+1} = u_{n+1}$. These equations are derived by substituting Eq. (2.17) into Eq. (2.16). So as to solve the above system of equations we have to split Eq. (2.18) at real and imaginary parts. As a result, we will have $2(n-1)$ real quadratic equations in $2(n-1)$ real variables.

Then, by having the final state $|\Phi\rangle$, the coin operators C_n can again be found by the definition of Eq. 2.14, except from the last (first) one C_1 . This happens because the state after the first step only satisfies the condition of Eq. (2.15) but not the one of Eq. (2.16) which is needed in the derivation of the coin operator.

The initial state $|\Psi^0\rangle = |1\rangle \otimes (u_{1,\uparrow}^{(0)} |1, \uparrow\rangle + u_{1,\downarrow}^{(0)} |1, \downarrow\rangle)$ and the first state $|\Psi^1\rangle = |1\rangle \otimes (u_{1,\uparrow}^{(1)} |1, \uparrow\rangle + u_{2,\downarrow}^{(1)} |1, \downarrow\rangle)$ after 0 and 1 step respectively, are both known. Thus, the coin operator C_1 can be calculated as

$$C_1 = \begin{bmatrix} u_{1,\uparrow}^{(1)} \\ u_{2,\downarrow}^{(1)} \end{bmatrix} \begin{bmatrix} u_{1,\uparrow}^{(0)} & u_{1,\downarrow}^{(0)} \end{bmatrix} \quad (2.19)$$

With the aforementioned algorithm, an arbitrary state over the walker's sites can be prepared (for an example, see Appendix B.1).

Combination of the two algorithms

We purpose to combine the two different algorithms for finding and preparing maximally entangled states. Implementing Reuver's algorithm, we find a state which maximizes the Schmidt norm. For example, for the simplest case, the state will have the form $|\psi\rangle = (\psi_{00}, \psi_{01}, \psi_{10}, \psi_{11})$. The quantum walk, as defined above Sec. 2.2.1, imposes some conditions on the initial site $i = 1$ and final site $i = n + 1$ of the walker, but the state over the internal sites $i = 2, n - 1$ could be arbitrary. The combination of both algorithms exploits exactly that freedom.

The idea is that one can impose the maximally entangled state found by Reuvers's algorithm at the internal sites $i = 2, n$ of the walker. Then, we just have to define the elements on the sites $i = 1$ and $i = n + 1$. They have the form $|site_1\rangle = u_{1,\uparrow} |1, \uparrow\rangle$ and $|site_{n+1}\rangle = u_{n+1,\downarrow} |n + 1, \downarrow\rangle$; since from the constraints (2.15) imposed to the state we have $u_{1,\downarrow} = 0$ and $u_{n+1,\uparrow} = 0$.

For example, after $n = 3$ steps the state has the following form

$$|\Psi\rangle = \begin{bmatrix} u_{1,\uparrow} & u_{2,\uparrow} & u_{3,\uparrow} & 0 \\ 0 & u_{2,\downarrow} & u_{3,\downarrow} & u_{4,\downarrow} \end{bmatrix} \quad (2.20)$$

Then, we have one more constraint coming from the orthogonality condition (2.16). After $n = 3$ steps, this constraint reads

$$u_{1,\uparrow}^* u_{2,\uparrow} + u_{2,\downarrow}^* u_{3,\downarrow} + u_{2,\uparrow}^* u_{3,\uparrow} + u_{3,\downarrow}^* u_{4,\downarrow} = 0 \quad (2.21)$$

We have one equation with two unknown variables; thus the system is under-determined and has a solution. Finally, after we fix the elements $u_{1,\uparrow}$ and $u_{n+1,\downarrow}$, we renormalise the state (for a numerical example, see Appendix B.2).

Therefore, in that way, the final state $|\Psi\rangle$ is determined and the "backward" quantum walk could be implemented to find the coin operators for the experimental preparation of the state.

2.2.2 Method B: Quantum walk with gradient descent techniques

The second approach aims to transform the above problem to an optimization problem. The algorithm will start with an arbitrary initial state and, by using the basin-hopping optimization technique, the free coin parameters of the quantum walk will be determined so that the output state will be a maximally entangled state.

The algorithm

We can implement the "forward" quantum walk by adding an optimization component to the algorithm. The only difference with the conventional quantum walk is the optimization component, which is realized with the minimization function, and the different definition of the coin operators. Each coin operator is a SU(2) matrix defined as

$$C_n = \begin{bmatrix} e^{i\zeta} \cos(\theta) & e^{i\zeta} \sin(\theta) \\ -e^{-i\zeta} \sin(\theta) & e^{-i\zeta} \cos(\theta) \end{bmatrix} \quad (2.22)$$

where θ, ζ, ξ are three independent and free parameters. The goal of the algorithm is to find the correct coin parameters of each coin operator in order to prepare the desired target state Φ . The algorithm that is used as the optimization component is the bashin-hopping algorithm.

For example, if we want to prepare a target state over $n + 1$ sites then we need n steps and n coin operators, which means $3 * n$ parameters to be determined.

We need to choose a function to be minimized or maximized. One could use *Fidelity*, *Schmidt norms*, *von Neumann entropy* [34] or any other property of the state. Then, the algorithm will find the correct coin operators to prepare the target state.

We test this when the function to be minimized is the $F = 1 - f(\Phi, \Phi')$, where Φ is the desired target state, Φ' the output state of the algorithm with the optimization component and $f(\Phi, \Phi') = \langle \Phi | \Phi' \rangle$ is the fidelity. The algorithm finds the correct coin parameters to minimize the f for small hilbert spaces. We will focus at the results at which the function to be minimized is the Schmidt norm.

The minimization function is defined as $F = norm - \sqrt{d}$, where $norm$ is the Schmidt norm computed numerically from Eq.(1.23) with $p = 1$, $k = \min(d_A, d_B)$ and \sqrt{d} is its maximum value, $d = \min(d_A, d_B)$.

As already underlined above, since subsystem A is always polarization of the single photon, we have $d_A = 2$ and, hence, $\sqrt{d} = \sqrt{2}$. On the contrary, we could choose the dimension of the subsystem B . For example, we could choose subsystem B to be the "internal" sites of the walker's sites in accordance with the previous discussion. Moreover, we could determine subsystem B over all sites of the walker's or arbitrary parts of it.

We should emphasize that the initial state will not affect the performance of the algorithm. For different initial states the algorithm will find different coin operators to arrive at a state that maximizes the Schmidt norm. Even with the same initial state there is more than one solution of the set of the coin parameters to maximize the Schmidt norm as we will see later.

The output of the algorithm are both Bell and high-dimensional maximally entangled states. We should underline that the algorithm is mainly useful for the preparation of high-dimensional maximally entangled states. Since, as it was explained in the Sec.2.1.2, the coin operators for the preparation of Bell states are trivial, given

that we start with the Bell state of Eq. (2.1).

Numerical results

Figure 2.5 shows the convergence of the algorithm after 2 steps of the quantum walk; the orbital angular momentum consists of three sites $m = -2, 0, 2$. The parameters n_{iter} , $n_{iter,success}$ and T were set to 10, 2 and 1 respectively. Around the 200 iterations and 400 iterations the algorithm gets stabilized to the maximum and then due to the parameter $n_{iter,success} = 2$ it stops.

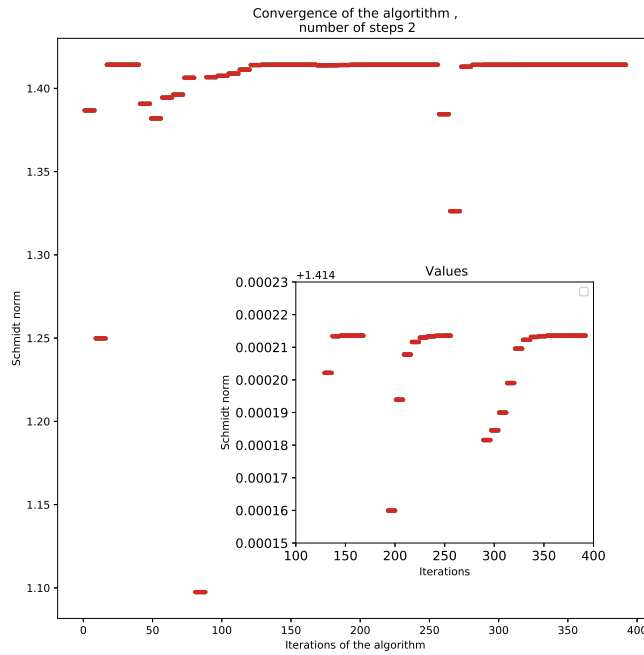


FIGURE 2.5: Result of the quantum walk algorithm with an optimization component for 2 steps.

Figure 2.6 shows the convergence of the algorithm after 9 steps of the quantum walk; the orbital angular momentum consists of ten sites $m = -9, -7, -5, -3, -1, 1, 3, 5, 7, 9$. The parameters n_{iter} , $n_{iter,success}$ and T were set to 10, 2 and 1 respectively. Around the 1200 and 1700 iterations at the figures 2.5 and 2.6 respectively, the algorithm gets stabilized to the maximum and then, once again, due to the parameter $n_{iter,success} = 2$ it stops.

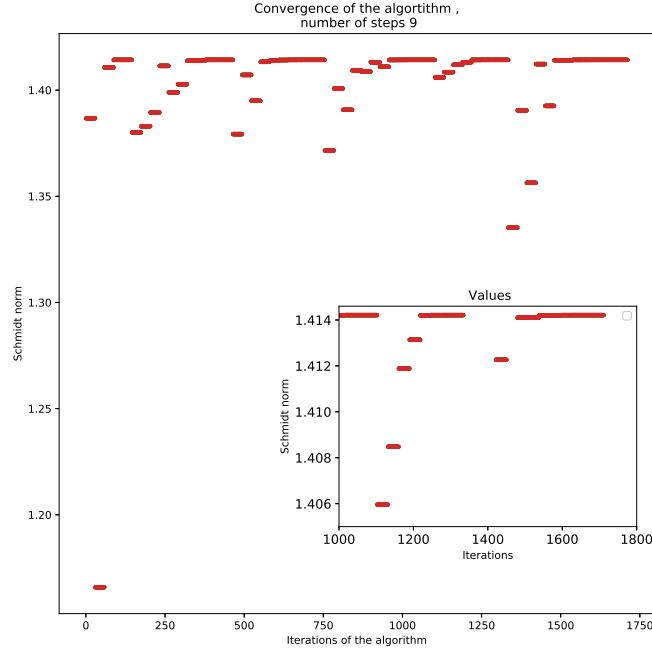


FIGURE 2.6: Result of the quantum walk algorithm with an optimization component for 9 steps.

As already discussed above, the importance of the algorithm is that it finds the coin operators for the preparation of high-dimensional maximally entangled states. For examples of such states see Appendix B.3.

Moreover, the algorithm also works for a higher-dimensional OAM Hilbert space, but the amplitudes are highly distributed over all sites with the result that the amplitudes of the more outer sites will be almost zero. In the case of ten sites, the amplitudes are significant at each OAM site and none of them could be considered zero (see example of a state at Appendix B.3). Moreover, ten sites are already a good illustration of a high-dimensional space, since a reasonable number of steps for photonic implementations is approximately 10 [5].

The algorithm allows one to also examine the case where the coin operators are not experimentally perfect. Specifically, we examine the cases where we have a constant dephasing parameter d (see Fig. 2.7 blue colour) and a random dephasing parameter d_i (see Fig. 2.7 orange colour) at all parameters θ_i . We choose the value of the parameter d equal to 1.3, while the parameter d_i is randomly selected from the number set 1.3 to 10.3 with step 1. In both cases, the algorithm finds the correct coin parameters to counteract the effect of the dephasing parameter. We observe that the number of iterations for the constant parameter are significantly smaller than the case of the random parameter. Once again the parameters used were : $n_{iter} = 10$, $n_{iter,success} = 2$ and $T = 1$.

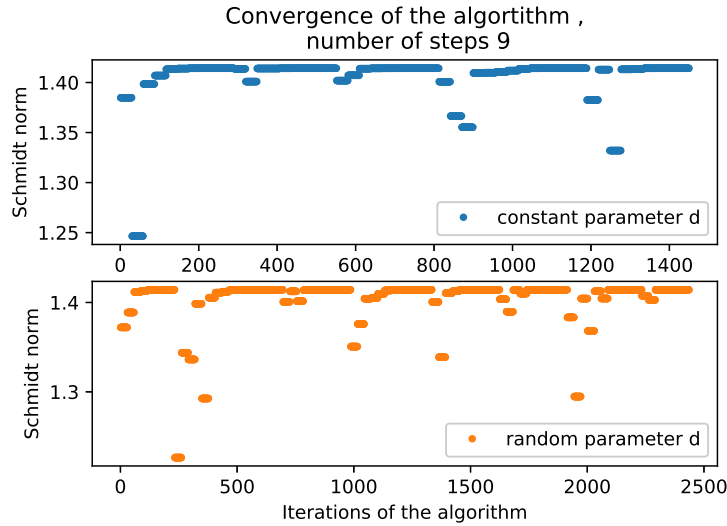


FIGURE 2.7: Convergence of the algorithm with a constant (blue colour) and random dephasing parametre d (orange colour).

2.3 Discussion

Possible experimental scheme Both methods could be implemented with the experimental scheme discussed in Sec.1.4. The coin operators and the measurement of the state for both methods will be realized in the same way already discussed in section 1.4; with a set of HWP-QWP and with projective measurements in SAM and SLM, for the coin and shift operators respectively. Method B, though, has a stronger connexion with experiments due to the shift operator; since the shift operator is the both-directional one can directly be implemented by choosing $\delta = \pi$, as was again explained in section 1.4. On the contrary, method A needs alterations in order to be experimentally implemented.

Comparison of method A and B Method A allows for the preparation of an arbitrary state compare to method B, which mainly enables the preparation of maximally entangled states. Even though, method B has a direct connexion with experiments as already mentioned above. The unidirectional shift operator used in method A, has the advantage of mathematical simplicity but lacks in the experimental implementation. Also, method B allows the consideration of defects in the experimental set up contrast to method A. Moreover, with method B one could explore more minimization functions and investigate the preparation of different states.

We should emphasize that method A prepares the desired target state in the internal sites of the whole state. Therefore, the target state is not directly approached compared to method B, where the target state is over all sites of the whole state. Also, the preparation of the state needs two more steps compared to method B; since the target state is over the internal sites. Moreover, method B allows the preparation of a desired state over specific sites of the whole state. One could just select the sites over which one to prepare the maximally entangled state and impose it as a condition in the algorithm.

Therefore, method B is more advantageous compared to method A.

Comparison of method B with related works We discussed in Sec.2.1.2 that Bell states over the external sites could easily be prepared with a quantum walk starting from a maximally entangled state. Method B is not affected by the initial state of the system, i.e any arbitrary state could be used as an initial state. Also, as mentioned above, it allows for the preparation of Bell states over different internal sites of the whole state.

More importantly, it allows for the preparation of high-dimensional maximally entangled states. We already discussed the importance of these states 2.1.1. Also, compared to the work of *Rigolin et. all.* [14], where a huge number of steps is needed for the preparation of maximally entangled states, method B is more advantageous. The number of steps scales linearly with the size of the OAM sites of the system, which is generally an asset when comes to photonic experimental schemes, as it is already discussed at section 1.4.

Chapter 3

Conclusions

In this work, we investigated the field of single-particle entanglement, and especially single-photon entanglement. We explored the preparation of these states with a quantum walk and exploited the SAM and OAM degrees of freedom of the single photon. Starting from an arbitrary state, localised in $m = 0$ site, we sought to find the correct coin operators for the preparation of the desired final state over $n + 1$ sites with n being the number of steps of the QW. By combining two different existing algorithms, we were able to find the coin operators (method A). But this method was lacking direct experimental realization due to the unidirectional shift operator. Therefore, we proposed a different algorithm where we use the both-directional shift operator (method B). Moreover, we transformed the problem into an optimization problem and we were able to find the correct coin operators for the realization of maximally entangled states in a single photon. The main advantage of method B, compared to method A and related work, is the direct experimental realization with a number of optical elements that scale linearly with the size of the state.

Significantly, we were able to prepare not only Bell states, but also high-dimensional maximally entangled states of a single photon by exploiting the large Hilbert space of the orbital angular momentum. Lately, intensive research is being done on high-dimensional states; since quantum information technologies will highly benefit from these states. Specifically with a single photon it will be possible to transfer a larger amount of information by taking advantage of both degrees of freedom and the high dimensionality. Also, CNOT gates for polarization and OAM degrees of freedom for a single photon are already realized experimentally. In addition with the single photon gates, they allow the experimental implementation of universal quantum computing with photonic technologies, where maximally entangled states will play an important role. Finally, teleportation of two qubits in a single photon simultaneously was recently implemented experimentally and, hence, the next step will be the teleportation of two qudits simultaneously.

Therefore, the preparation of high dimensional maximally entangled states experimentally is of highest importance, since it will be the first step for the aforementioned teleportation protocols and the implementation of many photonic quantum information technologies.

Appendix A

Appendix A : Proof of Reuvers's algorithm

We have defined the *Schmidt norms*

$$\| \psi \rangle \|_{p,k} = \left(\sum_{i=1}^k (\lambda_i^\Psi)^p \right)^{1/p} \quad (\text{A.1})$$

where $k \leq \min(d_A, d_B)$ and $p \geq 1$.

The author notes that $\| \psi \rangle \|_{p,k}^p$ is equal to

$$\| \psi \rangle \|_{p,k}^p = \langle \psi | \left(\sum_{i=1}^k (\lambda_i^\Psi)^{p-1} | \psi_A \rangle \otimes | \psi_B \rangle \right) \quad (\text{A.2})$$

which can be proved by doing the Schmidt decomposition of the state $\langle \psi |$ in the bipartite Hilbert space $| \psi \rangle \in H_A \otimes H_B$ with Schmidt coefficients λ_i^Ψ .

Then using the Cauchy-Schwarz inequality

$$| \langle u, v \rangle | \leq \| u \| \| v \| \quad (\text{A.3})$$

and that $\| \psi \rangle \| = 1$ we have

$$\| \psi \rangle \|_{p,k}^p \leq \langle \psi | \left(\sum_{i=1}^k (\lambda_i^\Psi)^{p-1} | \psi_A \rangle \otimes | \psi_B \rangle \right) \quad (\text{A.4})$$

$$\| \psi \rangle \|_{p,k}^p \leq \left\| \left(\sum_{i=1}^k (\lambda_i^\Psi)^{p-1} | \psi_A \rangle \otimes | \psi_B \rangle \right) \right\| \quad (\text{A.5})$$

From step 2 of the algorithm we have the equality

$$\left\| \left(\sum_{i=1}^k (\lambda_i^\Psi)^{p-1} | \psi_A \rangle \otimes | \psi_B \rangle \right) \right\| = \langle \varphi | \left(\sum_{i=1}^k (\lambda_i^\Psi)^{p-1} | \psi_A \rangle \otimes | \psi_B \rangle \right) \quad (\text{A.6})$$

Thus, eq.6.9 becomes

$$\| \psi \rangle \|_{p,k}^p \leq \left(\langle \varphi | \sum_{i=1}^k (\lambda_i^\Psi)^{p-1} | \psi_A \rangle \otimes | \psi_B \rangle \right) \quad (\text{A.7})$$

Then, we could Schmidt decompose the state $|\varphi\rangle$ in the bipartite Hilbert space $|\psi\rangle \in H_A \otimes H_B$ with Schmidt coefficients λ_i^φ and eq.6.7 becomes

$$\| |\psi\rangle \|_{p,k}^p \leq \left(\sum_{i=1}^k (\lambda_i^\Psi)^{p-1} \lambda_i^\varphi \right) \quad (\text{A.8})$$

Finally, we could use Holder's inequality

$$\sum_{i=1}^k |x_i y_i| \leq \left(\sum_{i=1}^k |x_i|^p \right)^{1/p} \left(\sum_{i=1}^k |y_i|^p \right)^{1/p} \quad (\text{A.9})$$

for all $(x_{k \in N}), (y_{k \in N}) \in C^N$ and p, q has to satisfy

$$1/p + 1/q = 1 \quad (\text{A.10})$$

Then, the right hand-side of eq.6.12 becomes

$$\left(\sum_{i=1}^k (\lambda_i^\Psi)^{p-1} \lambda_i^\varphi \right) \leq \left(\sum_{i=1}^k ((\lambda_i^\Psi)^{p-1})^q \right)^{1/q} \left(\sum_{i=1}^k (\lambda_i^\varphi)^p \right)^{1/p} \quad (\text{A.11})$$

and for eq. 6.14 to be valid $q = p/(p-1)$. Thus, eq. 6.15 becomes

$$\left(\sum_{i=1}^k (\lambda_i^\Psi)^{p-1} \lambda_i^\varphi \right) \leq \left(\sum_{i=1}^k (\lambda_i^\Psi)^p \right)^{\frac{p-1}{p}} \left(\sum_{i=1}^k (\lambda_i^\varphi)^p \right)^{1/p} = \| |\psi\rangle \|_{p,k}^{p-1} \| |\varphi\rangle \|_{p,k} \quad (\text{A.12})$$

where we applied eq.6.5 for the last step. From eq.6.12 and eq.6.16 we have

$$\| |\psi\rangle \|_{p,k}^p \leq \| |\psi\rangle \|_{p,k}^{p-1} \| |\varphi\rangle \|_{p,k} \quad (\text{A.13})$$

$$\Rightarrow \| |\psi\rangle \|_{p,k} \leq \| |\varphi\rangle \|_{p,k} \quad (\text{A.14})$$

This proves that at each step the *Schmidt norm* is increased, but the convergence is not guaranteed. This is also the reason why one of the two subsystems must remain two dimensional. At the case where H_A defines the smaller space of subspaces with dimension four, the algorithm has to be altered a bit, adding the following

$$|\psi\rangle := |\psi^{(2)}\rangle \wedge \dots \wedge |\psi^{(2)}\rangle = \frac{P |\psi^{(2)}\rangle \otimes \dots \otimes |\psi^{(2)}\rangle}{\| P |\psi^{(2)}\rangle \otimes \dots \otimes |\psi^{(2)}\rangle \|} \quad (\text{A.15})$$

where $|\psi^{(2)}\rangle := \sum_{i=1}^{d/2} \sqrt{2/d} |\psi_{2i-1}\rangle \wedge |\psi_{2i}\rangle$ [b3].

The complete proof for more general cases, are difficult to obtain, but [35] proposed a conjecture that could be helpful for generalizing the above theorem [21].

Appendix B

Appendix B : Numerical examples

B.1 Example of "backward" quantum walk

For implementing the "backward" quantum walk, we start from the state $|\phi\rangle = (1, 1, 1, 1)/2$, which is a balanced superposition over 4 sites. The initial state (superposition over 1 site) is known, for example we use the state $|\Psi^0\rangle = |1\rangle \otimes \frac{1}{\sqrt{2}}(|1, \uparrow\rangle + |1, \downarrow\rangle)$.

Then, we solve numerically the set of non-linear equations and we find the set of parameters $d_{i=2}^n$ to be $\{(i, 1 - i)/2\}$. Numerically we achieve that by using the *fsolve* function from the *scipy* library at *python*.

Next, we can define the final state Φ of the quantum walk using eq.(2.17) (not normalized -> Question : Is that a problem?)

$$\Phi = \frac{1}{2} (|1, \uparrow\rangle + (1 - i)|2, \uparrow\rangle + i|2, \downarrow\rangle + i|3, \uparrow\rangle + (1 - i)|3, \downarrow\rangle + |4, \downarrow\rangle) \quad (\text{B.1})$$

The coin operators are calculated from Eqs.(2.14) and (2.19).

B.2 Examples of Method A : combination of both algorithms

The Hilbert space $H \equiv H_A \otimes H_B$ has dimension $d = d_A * d_B$, where H_A refers to the 2-dimensional space of the spin angular momentum \uparrow, \downarrow and H_B to the k -dimensional space of the orbital angular momentum of the single photon .

B.2.1 Hilbert space of dimension 4

For the preparation of a maximally entangled state with a single photon, we need to have $d_B \geq 2$. The simplest case is when we have $d_B = 2$ and thus the dimension of the Hilbert space is $d = d_A * d_B = 4$. Then, the state reads

$$|\psi\rangle = \begin{bmatrix} u_{m_1, \uparrow} & u_{m_2, \uparrow} \\ u_{m_1, \downarrow} & u_{m_2, \downarrow} \end{bmatrix} \quad (\text{B.2})$$

For the preparation of that state with the quantum walk we need $d_B + 1 = 3$ number of steps, since at the initial and final sites we have constraints as explained above.

The maximally entangled state could be the well-known Bell states or the outputs of the Reuver's algorithm which are superposition of Bell states. For example,

$$|\psi\rangle = \begin{bmatrix} 0.6148 & 0.3492 \\ 0.3492 & -0.6148 \end{bmatrix} \quad (\text{B.3})$$

Then, as explained above we impose that state at the "inner" sites,

$$|\Psi\rangle = \begin{bmatrix} u_{1,\uparrow} & 0.6148 & 0.3492 & 0 \\ 0 & 0.3492 & -0.6148 & u_{4,\downarrow} \end{bmatrix} \quad (\text{B.4})$$

and find the values for the elements $u_{1,\uparrow}$ and $u_{4,\downarrow}$ that satisfy the orthogonality condition (2.21). In that case, we have $u_{1,\uparrow} = u_{4,\downarrow} = 0$. Thus, the state is

$$|\Psi\rangle = \begin{bmatrix} 0 & 0.6148 & 0.3492 & 0 \\ 0 & 0.3492 & -0.6148 & 0 \end{bmatrix} \quad (\text{B.5})$$

The state $|\Psi\rangle$ is the target state of the quantum walk over both the coin space and the walker's site, which is refereed at the previous sections as $|\Phi\rangle$. Then, the "backward" quantum walk can be implemented and find the coin operators for the preparation of the state.

$$C1, C2, C3 = \begin{bmatrix} 0 & 0.707 \\ 0.707 & 0 \end{bmatrix}, \begin{bmatrix} 0.349 & 0.615 \\ 0.615 & -0.345 \end{bmatrix}, \begin{bmatrix} 0.148 & 0.691 \\ -0.691 & -0.148 \end{bmatrix} \quad (\text{B.6})$$

where the initial state was chosen as $|\Psi^0\rangle = |1\rangle \otimes (0.209 |1, \uparrow\rangle + 0.978 |1, \downarrow\rangle)$. The choice of the initial state does not matter since the C_1 coin operator is defined as (2.19).

B.2.2 Hilbert space of higher dimensions

As an example for the higher dimensions case, I will discuss the case where $d_B = 4$, which means that we need $d_B + 1 = 5$ number of steps for the preparation of the state.

From the implementation of Reuvers's algorithm we have the following state as an output

$$|\psi\rangle = \begin{bmatrix} 0.526 & 0.276 & 0.261 & 0.251 \\ 0.229 & 0.484 & 0.321 & 0.355 \end{bmatrix} \quad (\text{B.7})$$

Then, we impose the state at the "inner" sites

$$|\Psi\rangle = \begin{bmatrix} u_{1,\uparrow} & 0.526 & 0.276 & 0.261 & 0.251 & 0 \\ 0 & 0.229 & 0.484 & 0.321 & 0.355 & u_{4,\downarrow} \end{bmatrix} \quad (\text{B.8})$$

and find the values for the elements $u_{1,\uparrow}$ and $u_{4,\downarrow}$ that satisfy the orthogonality condition (2.16). One possible solution is $u_{1,\uparrow} = 0.481$ and $u_{4,\downarrow} = 0.631$. After the renormalisation, the state reads

$$|\Psi\rangle = \begin{bmatrix} 0.377 & 0.412 & 0.216 & 0.204 & 0.197 & 0 \\ 0 & 0.179 & 0.379 & 0.252 & 0.278 & 0.494 \end{bmatrix} \quad (\text{B.9})$$

Then, we have the target state Φ and we can implement the "backward" quantum walk and find the coin operators for the preparation of the state.

$$C_1, C_2, C_3 = \begin{bmatrix} 0.557 & -0.291 \\ 0.265 & -0.731 \end{bmatrix}, \begin{bmatrix} 0.659 & 0.202 \\ -0.300 & 0.659 \end{bmatrix}, \begin{bmatrix} 0.693 & -0.195 \\ -0.015 & 0.693 \end{bmatrix} \quad (\text{B.10})$$

$$C_4, C_5 = \begin{bmatrix} 0.608 & 0.466 \\ -0.207 & -0.608 \end{bmatrix}, \begin{bmatrix} 0.316 & 0.632 \\ -0.316 & -0.632 \end{bmatrix} \quad (\text{B.11})$$

where the initial state was chosen as $|\Psi^0\rangle = |1\rangle \otimes (0.447 |0, \uparrow\rangle + 0.894 |0, \downarrow\rangle)$.

B.3 Examples of Method B : algorithm with optimazation component

We start from the localized state over one site $|\Psi^0\rangle = (0.5 |0, \uparrow\rangle + |0, \downarrow\rangle)$, we renormalize the state and after $n = 2$ and $n = 9$ steps, we arrive at the following maximally entnagled states

$$|\Psi_{\text{sites}=-2,2}\rangle = \begin{bmatrix} 0.000 & 0.000 & 0.231j & 0.000 & -0.352 - 0.613j \\ 0.548 - 0.446j & 0.000 & 0.009 - 0.021j & 0.000 & 0.000 \end{bmatrix} \quad (\text{B.12})$$

$$|\Psi_{\text{sites}=-9,-1}\rangle = \begin{bmatrix} 0.000 & 0.008 - 0.006j & 0.028 - 0.080j & -0.089 - 0.216j & -0.146 - 0.026j \\ -0.031 + 0.032j & -0.070 + 0.145j & 0.231 - 0.123j & -0.094 + 0.149j & -0.236 - 0.015j \end{bmatrix} \quad (\text{B.13})$$

$$|\Psi_{\text{sites}=1,9}\rangle = \begin{bmatrix} -0.118 - 0.116j & 0.439 + 0.179j & -0.367 - 0.099j & -0.122 + 0.071j & -0.011 + 0.014j \\ -0.358 - 0.338 & -0.267 - 0.0212j & -0.044 + 0.027j & -0.002 + 0.004j & 0.000 \end{bmatrix} \quad (\text{B.14})$$

The equations (B.13) and (B.14) refer to the state $|\Psi_{\text{sites}=-9,9}\rangle$, where the zero matrix elements (sites=-8,-6,-4,-2,0,2,4,6,8) have been eliminated. The Schmidt norm is equal to 1.414213 for both cases. Moreovoer, the coin operators needed are two and nine respectively and the coin parameters are $\theta_i, \xi_i, \zeta_i = \{8.129, 2.592, 6.841\}, \{4.979, 1.172, 3.121\}$ and $\theta_i, \xi_i, \zeta_i = \{5.438, 5.587, 8.823\}, \{2.363, 9.265, 4.381\}, \{8.723, 9.267, 5.959\}, \{3.875, 6.594, 3.501\}, \{3.355, 1.823, 0.858\}, \{1.091, 2.785, 8.783\}, \{8.686, 1.228, 0.097\}, \{2.485, 7.764, 8.413\}, \{1.147, 2.933, 8.013\}$ respectively.

Bibliography

1. Kempe, J. Quantum random walks: An introductory overview. *Contemporary Physics* **44**, 307–327 (2003).
2. Aharonov, Y., Davidovich, L. & Zagury, N. Quantum random walks. *Phys. Rev. A* **48**, 1687–1690 (2 1993).
3. Omar, Y., Sheridan, L. & Bose, S. Quantum walk on a line with two entangled particles. *Phys. Rev. A* **74**, 042304 (4 2006).
4. Flamini, F., Spagnolo, N. & Sciarrino, F. Photonic quantum information processing: a review. *arXiv: 1803.02790v2* (2018).
5. Cardano, F. *et al.* Detection of Zak phases and topological invariants in a chiral quantum walk of twisted photons. *Nature communications* **8**, 15516. ISSN: 2041-1723 (2017).
6. Cardano, F. *et al.* Quantum walks and wavepacket dynamics on a lattice with twisted photons. *Science Advances* **1** (2015).
7. Mohseni, M., Rebentrost, P., Lloyd, S. & Aspuru-Guzik, A. Environment-assisted quantum walks in photosynthetic energy transfer. *The Journal of Chemical Physics* **129**, 174106 (2008).
8. Shenvi, N., Kempe, J. & Whaley, K. B. Quantum random-walk search algorithm. *Phys. Rev. A* **67**, 052307 (5 2003).
9. Giri, P. R. & Korepin, V. E. A review on quantum search algorithms. *Quantum Information Processing* **16**, 315. ISSN: 1573-1332 (2017).
10. Childs, A. M. Universal Computation by Quantum Walk. *Phys. Rev. Lett.* **102**, 180501 (18 2009).
11. Lovett, N. B., Cooper, S., Everitt, M., Trevers, M. & Kendon, V. Universal quantum computation using the discrete-time quantum walk. *Phys. Rev. A* **81**, 042330 (4 2010).
12. Innocenti, L. *et al.* Quantum state engineering using one-dimensional discrete-time quantum walks. *Phys. Rev. A* **96**, 062326 (6 2017).
13. Zhang, P. *et al.* Implementation of one-dimensional quantum walks on spin-orbital angular momentum space of photons. *Phys. Rev. A* **81**, 052322 (5 2010).
14. Vieira, R., Amorim, E. P. M. & Rigolin, G. Dynamically Disordered Quantum Walk as a Maximal Entanglement Generator. *Phys. Rev. Lett.* **111**, 180503 (18 2013).
15. Chandrashekar, C. M., Srikanth, R. & Laflamme, R. Optimizing the discrete time quantum walk using a SU(2) coin. *Phys. Rev. A* **77**, 032326 (3 2008).
16. Misguish, G. *Quantum entanglement in condensed matter* (Lecture, CEA Saclay, 2015).
17. Bennett, C. *The Quantum Nature of Information* (Lecture, University of Edinburgh, 2013).

18. Krenn, M., Malik, M., Erhard, M. & Zeilinger, A. Orbital angular momentum of photons and the entanglement of Laguerre–Gaussian modes. *Philosophical Transactions of the Royal Society of London A: Mathematical, Physical and Engineering Sciences* **375**. ISSN: 1364-503X (2017).
19. Schmidt, E. Zur Theorie der linearen und nichtlinearen Integralgleichungen. I. Teil: Entwicklung willkürlicher Funktionen nach Systemen vorgeschriebener. *Mathematische Annalen* **63**, 433–476 (1907).
20. Peschel, I. Special Review: Entanglement in Solvable Many-Particle Models. *Brazilian Journal of Physics* **42**, 267–291. ISSN: 1678-4448 (2012).
21. Reuvers, R. An algorithm to explore entanglement in small systems. *Proceedings of the Royal Society of London A: Mathematical, Physical and Engineering Sciences* **474**. ISSN: 1364-5021 (2018).
22. Fletcher, R. *Practical methods of optimization* 2nd ed. ISBN: 978-0-471-49463-8 (Wiley, May 2000).
23. Kitagawa, T., Rudner, M. S., Berg, E. & Demler, E. Exploring topological phases with quantum walks. *Phys. Rev. A* **82**, 033429 (3 2010).
24. Groh, T. *et al.* Robustness of topologically protected edge states in quantum walk experiments with neutral atoms. *Phys. Rev. A* **94**, 013620 (1 2016).
25. Xiao, Y.-F., Zou, X.-B., Jiang, W., Chen, Y.-L. & Guo, G.-C. Analog to multiple electromagnetically induced transparency in all-optical drop-filter systems. *Phys. Rev. A* **75**, 063833 (6 2007).
26. Broome, M. A. *et al.* Discrete Single-Photon Quantum Walks with Tunable Decoherence. *Phys. Rev. Lett.* **104**, 153602 (15 2010).
27. Horodecki, R., Horodecki, P., Horodecki, M. & Horodecki, K. Quantum entanglement. *Rev. Mod. Phys.* **81**, 865–942 (2 2009).
28. Can, M. A., Klyachko, A. & Shumovsky, A. Single-particle entanglement. *Journal of Optics B: Quantum and Semiclassical Optics* **7**, L1 (2005).
29. Erhard, M., Fickler, R., Krenn, M. & Zeilinger, A. Twisted photons: new quantum perspectives in high dimensions. *Light: Science Amp; Applications* **7** (17146 2018).
30. Kim, Y.-H. Single-photon two-qubit entangled states: Preparation and measurement. *Phys. Rev. A* **67**, 040301 (4 2003).
31. J. H. Lopes W. C. Soares, B. L.B.D.P.C.A. C. Experimental realization of a quantum CNOT gate for orbital angular momentum and polarization with linear optical elements. *arXiv : 1807.06065* (2018).
32. Deng, L.-P., Wang, H. & Wang, K. Quantum CNOT gates with orbital angular momentum and polarization of single-photon quantum logic. *J. Opt. Soc. Am. B* **24**, 2517–2520 (2007).
33. Wang, X.-L. *et al.* Quantum teleportation of multiple degrees of freedom of a single photon. *Nature* **518** (7549 2015).
34. Nielsen, M. A. & Chuang, I. L. Quantum Computation and Quantum Information. *Cambridge University Press* (2003).
35. Yang, C. N. *J. Math. Phys.* 418–419 (4 1963).